Editors' Suggestion

Understanding the molecular origin of shear thinning in associative polymers through quantification of bond dissociation under shear

Irina Mahmad Rasid,[1] Jorge Ramirez,[2] Bradley D. Olsen,[3,*] and Niels Holten-Andersen[1,†]
[1]Department of Materials Science and Engineering, Massachusetts Institute of Technology, Cambridge, Massachusetts 02139, USA
[2]Department of Chemical Engineering, Universidad Politécnica de Madrid, Madrid, Spain
[3]Department of Chemical Engineering, Massachusetts Institute of Technology, Cambridge, Massachusetts 02139, USA

(Received 20 September 2019; accepted 27 February 2020; published 11 May 2020)

Understanding the physics of associative polymers is often limited by our inability to directly measure bond dissociation under deformation. In this work, we developed a rheo-fluorescence technique and applied it to characterize the nonlinear shear response of linear side-functionalized polymer chains cross-linked via nickel-terpyridine complexation. As the network was sheared, the fraction of dissociated bonds was quantitatively measured based upon a change in fluorescence with metal dissociation. Shear thinning of the gel was accompanied by only a small increase in the fraction of dissociated bonds. Comparison with several transient network models shows that the shear thinning within the constraint of the measured fraction of dissociated bonds cannot be explained by classical theories that include retraction of dangling chains alone; the rheological response likely involves alternative modes of stress relaxation.

DOI: 10.1103/PhysRevMaterials.4.055602

I. INTRODUCTION

Inspired by natural materials, associative polymer gels have in recent years become an increasingly popular choice in the design of soft synthetic materials for a range of applications that require high toughness and complex flow properties [1–10]. Newly developed design strategies allow the mechanical properties and time-dependent behaviors of these gels to be tuned and take advantage of the gels' diverse rheological behavior, including shear thinning, shear thickening and self-healing [11–14]. However, understanding the molecular mechanisms responsible for these properties remains challenging.

The development of constitutive models has provided theoretical insight into the dynamics and flow behavior of transient networks. Most of these theories are able to reproduce the key features of experimental observations on transient networks. However, the large number of adjustable parameters in the theories makes a quantitative evaluation of their predictions difficult [15,16]. Therefore, while it is generally agreed that force-induced dissociation of bonds is critical for shear thinning [17–26], the details of the physics remain unclear. Most earlier work attributed shear thinning to the retraction of the ejected chains due to the entropic spring force acting on them, reducing the stress in the network. A common feature of these models is their prediction that the fraction of dissociated bonds increases significantly when the material is sheared [17–23]. More recent work suggests that other events, including the formation of elastically inactive loops [25] or the development of spatial heterogeneity in the network [26], can yield a similar degree of shear thinning without a large change in the fraction of dissociated bonds. As a result, direct measurement of the number of dissociated bonds in a transient network during shear flow is needed to critically evaluate the predictions of these theories. To address this challenge, this work quantitatively measures force-induced bond dissociation in a model associative polymer gel as a function of the applied shear strain under steady shear flow using a newly developed rheo-fluorescence instrument, and it compares the results of the measurements with transient network theory, providing substantial insight into the molecular origin of shear thinning in associative polymers.

II. MATERIALS AND METHODS

A. Materials

Reagents 4′-chloro-2, 2′ : 6′, 2″-terpyridine, 98% and 3-amino-1-propanol were purchased from Alfa Aesar. Potassium hydroxide (KOH) was purchased from VWR. Methacryloyl chloride (with 200 ppm monomethyl ether hydroquinone as stabilizer), triethylamine, *N*,*N*-dimethylacrylamide (with 500 ppm monomethyl ether hydroquinone as inhibitor), 2, 2′-azobisisobutyronitrile (98%), dimethyl sulfoxide (anhydrous), dichloromethane (anhydrous), and *N*,*N*-dimethylacetamide were purchased from Sigma-Aldrich. 2-([(ethylthio)carbonothioyl]thio)-2-methylpropanoic acid (EMP) was synthesized as described previously (^{1}H NMR spectrum in Fig. S1) [27]. *N*,*N*-dimethylacrylamide (DMA) was purified through a basic alumina column to remove inhibitor before polymerization. All other chemical reagents were purchased from Sigma-Aldrich or VWR and used as received.

B. Characterizations

NMR spectra were recorded on a Mercury 300 MHz spectrometer. The residual undeuterated solvent peaks were

*bdolsen@mit.edu
†holten@mit.edu

used as references [7.27 ppm for $CDCl_3$ and 3.30 ppm for $(CD_3)(_2SO)$]. Gel permeation chromatography (GPC) measurements were performed on an Agilent 1260 LC system with two ResiPore columns (300 × 7.5 mm, Agilent Technologies, Santa Clara, CA) in series at a flow rate of 1 mL/min at 60 °C, where DMF with 10% triethylamine and 10% pyridine was used as the mobile phase. The molar masses were determined using a Wyatt miniDAWN TREOS multiangle light scattering detector and a Wyatt Optilab T-rEX differential refractive index detector. Liquid chromatography-mass spectrometry (LC-MS) analysis was performed using an Agilent 1260 Infinity LC system coupled with a 6130 quadrupole mass spectrometer. A mixture of 0.1% formic acid in water and MeCN was used as the mobile phase.

1. Synthesis of 3-([2, 2′ : 6′, 2″-terpyridin]-4′-yloxy)-propan-1-amine (I)

To a stirred suspension of 3.05 g (2.4 equi., 45.2 mM) of powdered KOH in 224 mL DMSO (in a flame-dried flask) at 40 °C, 6 mL (4.4 equi., 81.7 mM) of 3-amino-1-propanol was added dropwise. After 20 min, under N_2 protection, 5.0 g (1 equi., 18.7 mM) of 4′-chloro-2, 2′ : 6′, 2′-terpyridine was added. The mixture was stirred at 40 °C for 2.5 h and then poured into deionized water. It was then placed in the −20 °C freezer overnight, after which a light yellow cloudy suspension forms. The aqueous phase was removed by vacuum filtration, and the product was washed with deionized water and vacuum-dried at 80 °C overnight, yielding 3.8 g of a light yellow solid. The filtrate was placed back in the −20 °C freezer and left overnight again, from which a further 0.8 g was recovered. (Yield: 4.6 g, 81%.) ^{1}H NMR (300 MHz, $CDCl_3$) δ 8.68 (ddd, J = 4.8, 1.8, 0.9 Hz, 1H), 8.60 (dt, J = 7.9, 1.1 Hz, 1H), 8.01 (s, 1H), 7.84 (td, J = 7.7, 1.8 Hz, 1H), 7.32 (ddd, J = 7.5, 4.8, 1.2 Hz, 1H), 4.32 (t, J = 6.1 Hz, 1H), 2.97 (t, J = 6.8 Hz, 1H), 2.02 (p, J = 6.4 Hz, 1H) (Fig. S2). LRMS (ESI) m/z calculated for C18H18N4O $[M+H]^+$ 307.1; found 307.1.

2. Synthesis of N-[3-([2, 2′ : 6′, 2″-terpyridin]-4′-yloxy)-propyl]methacrylamide (II)

The reaction vessel and addition funnel were first flame-dried and purged with dry nitrogen three times. Under nitrogen flow, 250 mg (1 equiv., 0.82 mM) of 4′-(3-hydroxypropoxy)-2, 2′ : 6′, 2″-terpyridine was dissolved with 0.14 mL triethylamine in 6.24 mL of dry DCM. This was then left stirring in an ice bath for 30 min to cool the solution down to 0 °C. Diluted with 1 mL DCM, 0.1 mL of methacryloyl chloride (1.25 equiv., 1.02 mM) was added dropwise using an addition funnel while stirring at 0 °C (ice bath). After 2 h, the cooling bath was removed, and the reaction mixture was stirred overnight. The next day, the solution appeared light yellow and cloudy. The solution was diluted with 10 mL of DCM, transferred into a separation funnel, and then washed twice with saturated sodium bicarbonate solution and once with Milli-Q water. The organic phase was isolated and dried over anhydrous sodium sulfate. The solvent was removed under reduced pressure at 30 °C. The residue was purified using silica flash chromatography with a gradient of 75% hexane:25% ethyl acetate to 100% ethyl acetate. After evaporation of the solvent, 194.4 mg (62.7% yield) of N-[3-([2, 2′ : 6′, 2″-terpyridin]-4′-yloxy)propyl]methacrylamide was obtained as a white powder. ^{1}H NMR (300 MHz, $CDCl_3$) δ 8.75–8.60 (m, 4H), 8.07 (s, 2H), 7.89 (t, J = 7.7 Hz, 2H), 7.43–7.32 (m, 2H), 5.75 (s, 1H), 5.39–5.30 (m, 1H), 4.39 (t, J = 5.9 Hz, 2H), 3.58 (q, J = 6.2 Hz, 2H), 2.16 (q, J = 6.1 Hz, 2H), 1.99 (dd, J = 1.6, 0.9 Hz, 3H) (Fig. S3). LRMS (ESI) m/z calculated for C22H22N4O2 $[M + H]^+$ 375.1; found 375.1.

3. Synthesis of Poly(DMA-co-Terpyridyl-Methacrylamide) [P(DMA-co-TpyMA)] (III)

Random copolymers from DMA and II were synthesized by reversible addition-fragmentation chain transfer (RAFT) polymerization (Fig. 1). The total monomer concentration in polymerization was 2.0 M, and the ratio of DMA/1/EMP/AIBN was 181:8:1:0.2. Polymerization was performed in DMAc at 70 °C for 12 h, and the reaction was quenched by exposure to air and cooling to room temperature. Polymers were purified by precipitation into diethyl ether and dried under vacuum. This monomer pair was chosen because previous work by others has shown that the product of the reactivity ratios for acrylamide and methacrylamide is close to unity [28,29]. Therefore, it was expected that the two monomers were copolymerized in a nearly statistical manner, and the terpyridine-functionalized monomer was evenly distributed along the polymer backbone. The mole fraction of the functionalized monomer in the polymer was 4.2%, determined by ^{1}H NMR (Fig. S4), close to the feed ratio of 4.4%. The molecular weight of the polymer was 17.4 kg mol^{-1}, as characterized by DMF GPC (Fig. S5). Yield: 9.4 g. The targeted conversion was 80%, and the actual conversion was calculated at 83%, from a comparison to the molecular weight (20.9 kg mol^{-1}) and mass of polymer (11.2 g) for 100% conversion.

4. Preparation of P(DMA-co-TpyMA)-nickel gels

In an Eppendorf tube, 100 mg of the polymer is first dissolved in 778 μL Milli-Q water, to which 222 μL of 100 mM $NiCl_2$ stock solution is added. The gel is then mixed vigorously with a PTFE-lined microspatula and centrifuged at 21 100g for 5 min to remove air bubbles.

5. Rheology

Stress relaxation and frequency sweep experiments were performed on an Anton Paar 301 Physica rheometer using a custom-made sapphire parallel plate upper geometry (50 mm in diameter, 3 mm in thickness). The plate was mounted onto a standard issue 10 mm disposable geometry with no further modifications, thus allowing it to be used with the MCR 301 (see Table S1, p. 7 for part numbers). Inertial calibration and motor adjustment were performed before each measurement. Hydrogel samples were centrifuged at 21 100g for 10 min at room temperature to remove bubbles before loading onto the rheometer. Mineral oil was added to the sample edge to minimize dehydration. Experiments were performed at 70, 75, and 80 °C, where the temperature was controlled by a Peltier plate. Stress relaxation and frequency sweep experiments were performed at 1% strain, which was within the

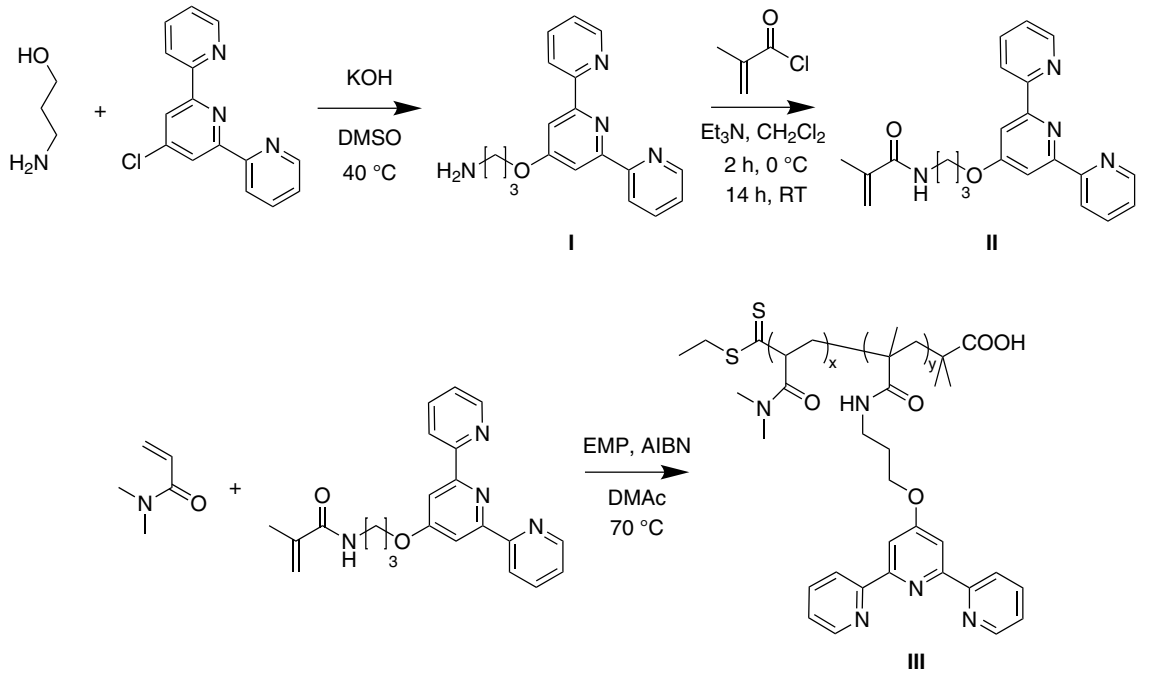

FIG. 1. Reaction scheme for the synthesis of the terpyridine-functionalized monomer (II) and P(DMA-co-TpyMA), where $x = 148$ and $y = 7$ as determined by ^{1}H NMR.

linear viscoelastic (LVE) region as determined by strain sweep experiments.

6. *Rheo-fluorescence setup*

Simultaneous measurement of the steady shear response and change in fluorescence of the gel was performed using a custom-built rheo-fluorescence setup designed to fit an Anton-Paar MCR 301 rheometer (Fig. 2). A UV LED with a peak wavelength of 340 nm was collimated with a UV grade AR-coated lens and passed through a short-pass filter (390 nm) to minimize the background signal from the excitation source itself. The collimated beam was then focused onto the sample through a transparent sapphire plate (50 mm in diameter, 3 mm in thickness). The plate was mounted onto a 10 mm plate disposable geometry, allowing it to be connected to the MCR drive. Sapphire provides both high UV transmission (>80%) and low autofluorescence (from impurities in the crystal) in the range 400–500 nm. Crystals that autofluoresce in this range, such as quartz, result in the saturation of the detector signal, while non-UV grade glass would have transmission as low as 50% at the excitation wavelength. A lens positioned above the plate collects fluorescent light, with a bandpass filter (451 ± 106 nm) limiting noise and background in the measurement. The height of the lens was adjusted to maximize light captured by a femtowatt

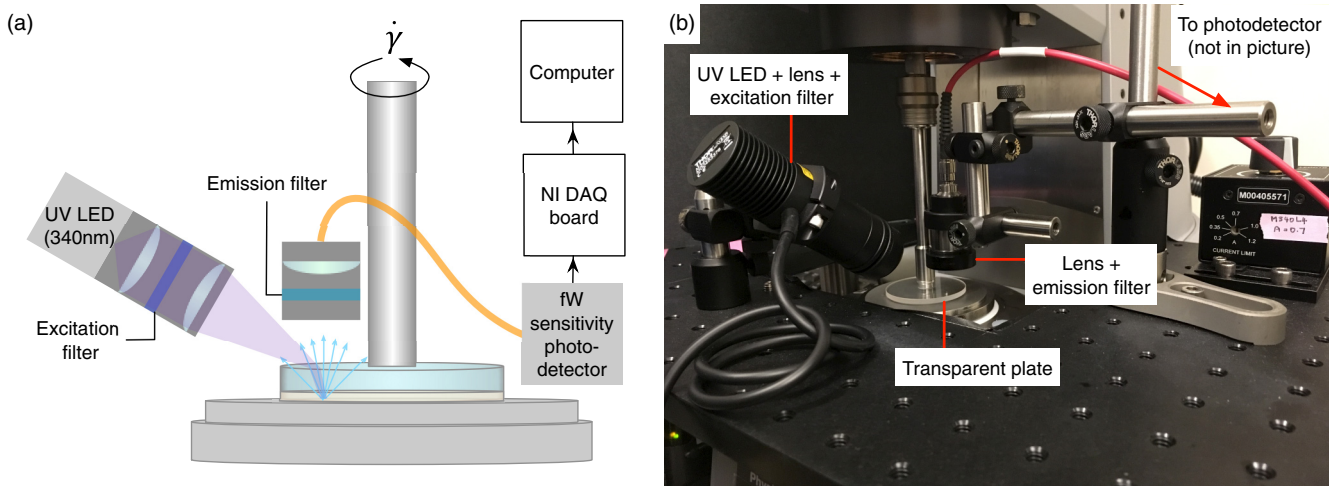

FIG. 2. (a) Schematic of the rheo-fluorescence setup showing the position of the excitation source and collection lens, relative to the transparent upper plate. (b) The photo shows the rheo-fluorescence setup, with the optical elements mounted on a raised breadboard.

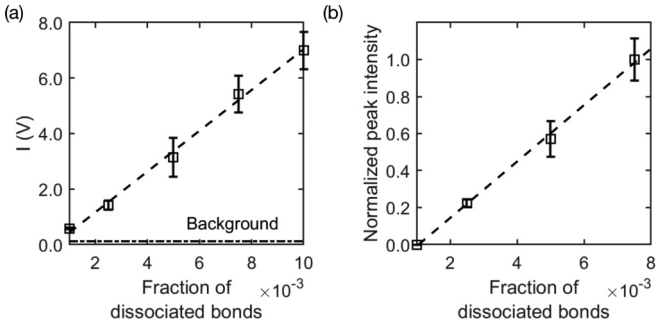

FIG. 3. (a) The calibration curve for calculating the fraction of dissociated bond from the measured photodetector output, obtained using standard solutions of known concentrations of terpyridine, at a gap height of 0.3 mm. (b) The fluorescence of the standard solutions was also measured on a fluorimeter, which supports the linear relation between the measured signal and the concentration.

photodetector. Connecting the detector and the collector lens via a fiber optic cable allows the lens to be positioned as close as possible to the upper plate of the rheometer. Crucially, this setup maintains the sampling volume constant throughout the experiment, allowing accurate measurement of the fraction of dissociated bonds f_d. Photodetector output is calibrated to determine the number of fluorescent groups as a function of signal. A complete parts list (Table S1, p. 7) can be found in the Supplemental Material [30].

The calibration of the rheo-fluorescence setup was performed with dilute solutions of the terpyridine-functionalized polymer of known concentrations. Since no metal ions are added, the concentration of terpyridine in the solution can be calculated from the concentration of the polymer in solution and the relative mole fraction of terpyridine as measured by ^{1}H NMR (see calculation details in Sec. F of the Supplemental Material) [30]. The solutions with known concentration of terpyridine are added to the lower plate, and the sapphire plate is then lowered to a gap height of 0.3 mm. The photodetector output for each concentration is recorded, and the resulting calibration curve is shown in Fig. 3(a). Since the setup consists of a parallel plate geometry, the experiment can be conducted at different gap heights. Thus, the gap height is also varied during the calibration process so that the appropriate correction can be applied in the calculation of the fraction of dissociated bonds for each experiment. The fluorescence of the standard solutions was also measured on a fluorimeter, which supports the linear relation between the measured signal and the concentration [Fig. 3(b)].

With parallel plates, the shear rate $\dot{\gamma}$ is a function of radial distance from the center of the plate. Thus, the sampling position was kept constant for all experiments and was always positioned as close to the edge as possible. The excitation beam was 5 mm in diameter, and the reported shear rate is the average $\dot{\gamma}$ across the irradiated area.

III. RESULTS AND DISCUSSION

To perform this measurement, a model system was developed where the transient bonds fluoresce when they are dissociated and are quenched when they are associated. The

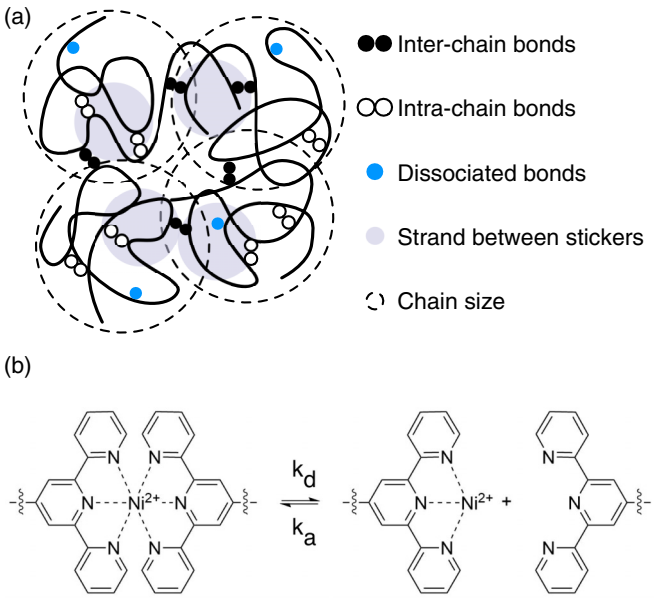

FIG. 4. (a) The proposed network structure of the gel consists of inter (bridging) and intra (loop) chain bonds, along with dissociated (dangling) bonds. Dangling chains may exist as both terminal chains or larger dangling segments between two physical junctions. The large circles denote the pervaded volume of the chains, which are overlapping, while the small gray circles indicate the pervaded volume for strand between stickers. (b) The bonds are bis complexes of terpyridine with nickel that form through a reversible reaction with rate constants, k_d and k_a.

model polymer network is a metal-coordinate gel, formed through the complexation of linear terpyridine-functionalized chains with nickel ions (Fig. 4). In its dissociated state, terpyridine fluoresces with an emission peak centered at 450 nm. With the addition of nickel ions, terpyridine forms quenched bis complexes with equilibrium constant $K_{\text{eq}} = k_d/k_a = 9 \times 10^{-5}$ [31], where k_d and k_a are the rate constants for dissociation and association, respectively. The quenched metal complexes have no fluorescence and little optical absorption [32]; therefore, the emission of the gel under steady shear is a direct measure of the number of dissociated terpyridine groups [30]. Terpyridine side functionalities were incorporated into a random copolymer of dimethyl acrylamide, synthesized by reversible addition-fragmentation chain transfer (RAFT) polymerization, with a molecular weight of 17.4 kg mol^{-1} and dispersity of 1.08. The polymer is estimated to have seven terpyridines per chain. Gels were prepared at 10% (w/v), which is above the gelation concentration, $\psi_{\text{gelation}} = 3.6\%$ (w/v), but below the entanglement concentration, $\psi_{\text{entanglement}} = 50\%$ (w/v) (Table S2, p. 9) [30]. The concentration for overlap of segments between the associating groups is estimated to be $\sim$12% (w/v). This value is close to the concentration of the gel used in this work, which implies that a significant number of the bonds will be formed within the chain itself. Combined with the small equilibrium constant, the quiescent network is expected to consist of a mixture of inter- and intrachain bonds, along with a small fraction of dissociated bonds (Fig. 4) [33].

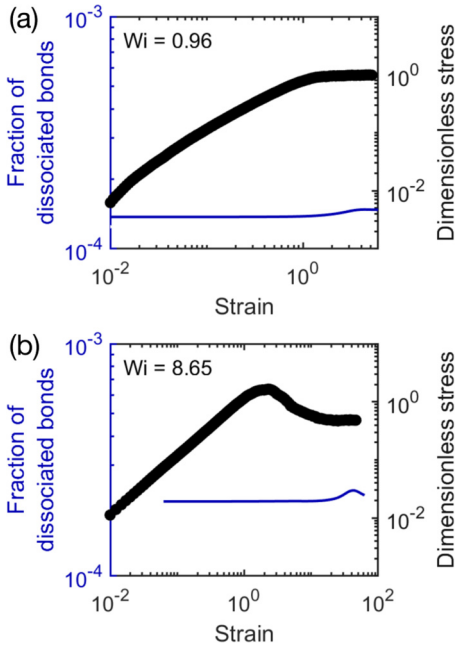

FIG. 5. Typical result from startup to steady shear experiments showing the change in the fraction of dissociated bonds f_d and dimensionless stress $\tilde{\sigma}$ as a function of strain for two shear rates: (a) $\mathrm{Wi} = 0.96$ and (b) $\mathrm{Wi} = 8.65$, where $\mathrm{Wi} = \dot{\gamma}\tau_r$. The f_d are smoothing spline fits applied to filter out the inherent noise from the photodetector.

The nonlinear response of the gel was captured through startup to steady shear measurements. The fluorescence of the gel was recorded throughout the experiment, from which f_d as a function of time and hence the applied strain can be quantified. Typical results are shown for two shear rates in Fig. 5, where f_d and dimensionless stress and $\tilde{\sigma}$ is plotted as a function of strain. The long-time asymptotes of the startup curves then give the steady-state response, which is shown in Figs. 6(d)–6(f) as a plot of normalized viscosity, $\eta = \tilde{\sigma}/\mathrm{Wi}$, as a function of $\mathrm{Wi} = \dot{\gamma}\tau_r$. τ_r is the network relaxation time, as measured from stress relaxation after a small step strain within the linear viscoelastic regime. The stress relaxation modulus decays with time and can be fit to a phenomenological Kohlrausch-Williams-Watts (KWW) function (Fig. 7), from which τ_r can be extracted (Table I). The β exponent is approximately 0.85 for the three temperatures tested, indicating that there is a spectrum of relaxation times, likely due to heterogeneity in the molecular weight and sticker distribution [34,35] and the sticky Rouse relaxation spectrum [33,36].

Terpy-acrylamide gels exhibit shear thinning across the entire range of shear conditions considered, consistent with structurally similar polymers [37,38], and they show a steady increase in the fraction of dissociated bonds with increasing shear rates within the error of the measurement [Figs. 6(a)–6(f)]. This observation of increasing f_d is consistent with the prediction of force-induced bond dissociation to accompany the shear thinning behavior. However, while the normalized viscosity exhibited a two orders of magnitude decrease for all three temperatures, f_d never exceeded 3×10^{-4}. No signs of heterogeneous flows were observed in additional experiments with variable gap height and experimental time, suggesting that these results are representative of a homogeneous flow in the material [30]. Therefore, shear

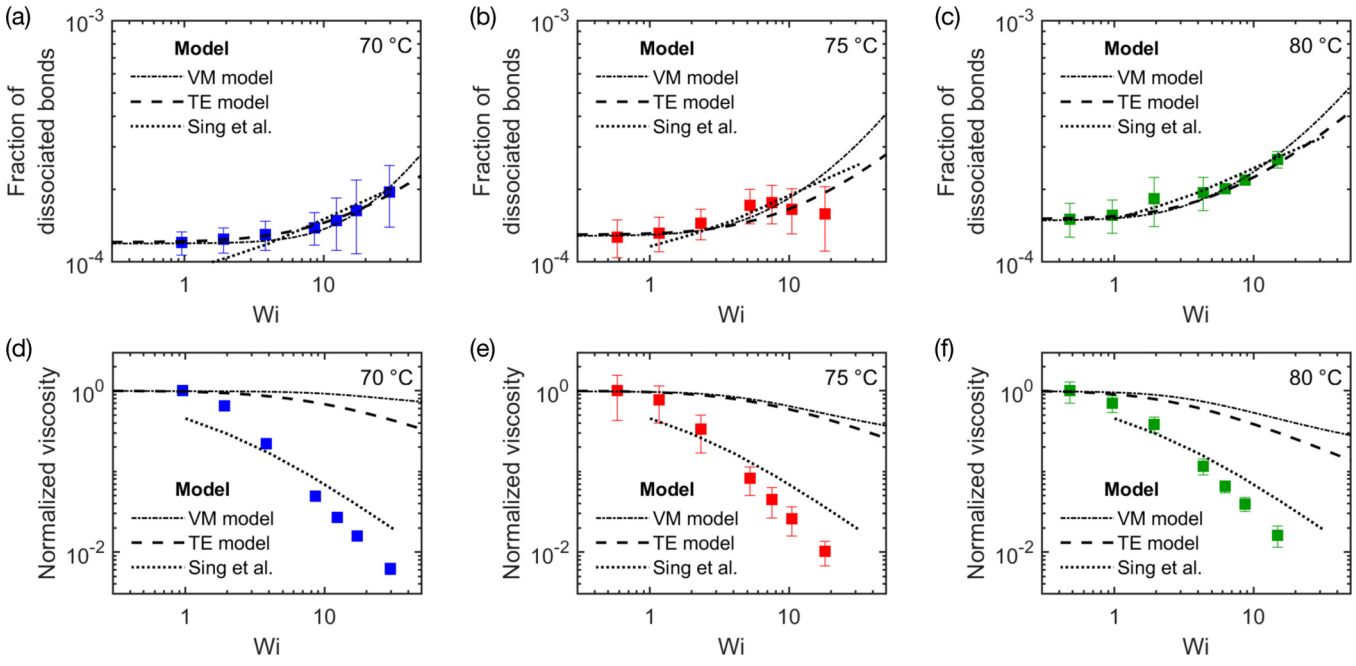

FIG. 6. (a)–(c) Best fits for the VM, TE, and Sing model obtained using least-squares fit by treating the parameters of the models as fitting parameters for data obtained at 70, 75, and 80 °C, respectively. (d)–(f) The corresponding η calculated for VM, TE, and Sing models, using the same fitting parameters, compared to data obtained at 70, 75, and 80 °C.

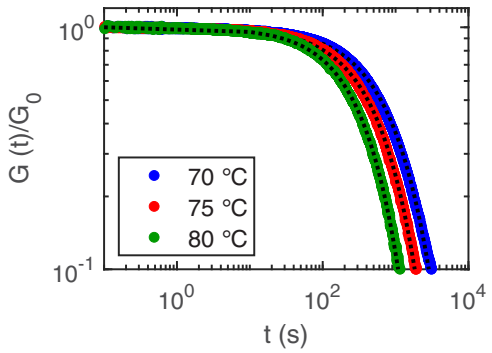

FIG. 7. Normalized stress relaxation following a small step strain (strain = 1%) at 70, 75, and 80 °C for the terpy-acrylamide gel. The dotted lines are fits to a phenomenological Kohlrausch-Williams-Watts (KWW) function.

thinning in this system occurs in the absence of large-scale bond dissociation.

In the following discussion, the terms "bridging," "loop," and "dangling chains" will be used to refer to the different states of the chain segments. These states correspond to the cases where the associating groups are participating in interchain bonds, participating in intrachain bonds, and are in a dissociated state, respectively. Dangling chains may exist as both terminal chains or larger dangling segments between two physical junctions, as illustrated in Fig. 4(a). Measuring the fraction of dissociated bonds provides direct quantification of the dangling chain fraction since this is the only fraction that is not fully associated. While the associative polymer used in this study was a linear side-functionalized chain, most models from transient network theory are based on telechelic systems, where chain dynamics are simpler to capture. Indeed, the challenges associated with capturing the behavior of linear side-functionalized chains are apparent from the fact that the models developed specifically for this chain architecture like sticky Rouse and sticky reptation have been limited to the prediction of the polymers' linear rheology properties and have not been extended to the nonlinear regime [33,36]. However, for the system considered here with few stickers and intrachain loop formation further reducing the effective functionality, telechelic models form a reasonable starting point for comparison.

Several modes of stress relaxation have been proposed by different models in transient network theory. A key difference in these models is the method used for obtaining the chain extension, which is required to compute the stress in the system. Most models, including those of Tanaka and Edwards (TE model) [17–20] and Vaccaro and Marrucci (VM model) [23], use the average chain extension, and these models attribute shear thinning to the detachment and subsequent retraction of dangling chains. In recent work by Sing *et al.* [25], the Smoluchowski equation was solved to model the entire distribution of chain extension for both bridging and dangling chains under steady shear flow for a range of equilibrium constants. At large enough shear rates, dangling chains were predicted to be more extended than bridging chains, indicating that chain retraction may not be the dominant mechanism for stress relaxation. Random diffusion of dangling chain ends

TABLE I. τ_r extracted from fitting the stress relaxation data to a phenomenological Kohlrausch-Williams-Watts (KWW) function.

T (°C)	τ_r (s)	β
70	959.5	0.85
75	642.6	0.86
80	586.8	0.84

may lead to diffusion of the chain from an extending to a retracting streamline, resulting in a net rotational flux of chain ends that is referred to as chain tumbling. Unlike all previous models, the fraction of loops was not assumed to be constant by Sing *et al.*, since calculation of the full chain distribution enabled the probability of loop and bridge formation to be calculated.

Comparisons to transient network theory suggest that modes of stress relaxation beyond chain detachment from physical cross-links are involved in the shear thinning behavior observed. To model experimental data for the terpy-acrylamide system, the parameters of each of these three models were treated as fitting parameters, and the best fit to f_d was first obtained using a least-squares method [Figs. 6(a)–6(c)]. The fit parameters were then used to calculate the predicted flow curve for each model [Figs. 6(d)–6(f)], and the difference between the predicted and experimental data is discussed in this context. While good fits were obtained for f_d, the predicted η is overestimated in the order of VM > TE > Sing. As seen in Figs. 6(d)–6(f), the model proposed by Sing *et al.* gives the closest approximation to the measured η under the constraint that the fraction of dissociated bonds must remain small. While the current experiment is unable to differentiate loops and bridges and therefore cannot fully test Sing's model, this result provides support for alternative modes of stress relaxation (loop formation, chain tumbling) beyond partial (VM model) or complete (TE model) retraction of dangling chains in the flow field.

Alternatively, the fit parameters can be obtained by first fitting the η data, from which the predicted f_d for the VM and TE model is calculated (Fig. S6). This approach shows that both models are unable to predict the degree of shear thinning observed even as f_d approached 1 for the TE model and $f_d > 20\%$ for the VM model, also indicating that retraction of dangling chains alone is insufficient to account for the shear thinning behavior.

The effect of temperature on the shear thinning behavior can be explained by the temperature dependence of the equilibrium constant of the gel. From the plot of f_d as a function of shear rate in Figs. 6(a)–6(c), it is apparent that increasing the temperature from 70 °C to 80 °C has the effect of shifting the curve up. This increase in f_d is small, in the order of 10^{-4} across the temperature range tested. The shear thinning behavior appears very similar, with η also showing a very small decrease with temperature [Figs. 6(d)–6(f)].

The shift up with temperature for f_d is consistent with a larger fraction of dissociated bond in the quiescent state at higher temperatures, as expected from the temperate dependence of K_{eq}. The activation energies for the association and dissociation of nickel-terpyridine bis complexes are

TABLE II. The probability rate of bond dissociation and association for a range of models.[a]

Author	Rate of bond association, p	Rate of bond dissociation, q
Tanaka and Edwards	p_0	$q_0 + 1.5q_1(r^2/\langle r^2\rangle_0)$
Vaccaro and Marrucci	$p_0 + p_1(r/\sqrt{\langle r^2\rangle_0})$	$q_0/(1 - r^2/L)$
Sing *et al.*	$p_0[1 - \exp(-4r^2/\langle r^2\rangle_0^2)]$	$q_0\exp(\tilde{q}\lvert(3kT/\langle r^2\rangle_0)\{r/[1 - (r/L)^2]\}\rvert)$

[a] p_0 and q_0 are the rate of bond association and dissociation at equilibrium, respectively, r is the chain extension, $\langle r^2\rangle_0$ is the average end-to-end distance for Gaussian chains, L is the contour length of the chain, k is the Boltzmann constant, T is the temperature, and q_1, p_1, $\tilde{q}$, and χ are model-specific constants.

$E_{a,\text{association}} = 12.1$ J mol^{-1} and $E_{a,\text{dissociation}} = 20.8$ J mol^{-1}, respectively [31], such that K_{eq} effectively increases with temperature, shifting the equilibrium to favor bond dissociation. The rates of bond dissociation and association for the three models are summarized in Table II. q_0 and p_0 in these expressions are analogous to k_d and k_a, respectively, as measured within the network environment. Fits of similar quality [Figs. 6(a)–6(f)] for the three models were obtained for increasing values of q_0/p_0 with temperature (Fig. 8), consistent with the interpretation of an increase in the probability of the bonds existing in the dissociated state.

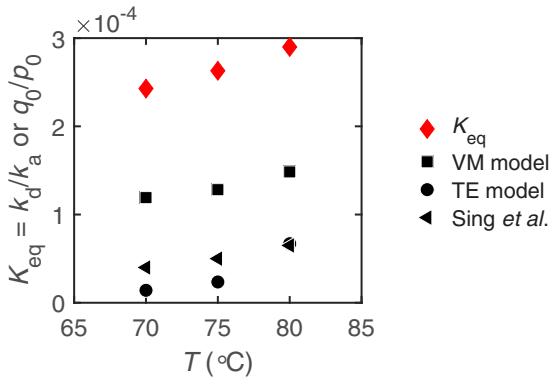

FIG. 8. Effect of temperature on K_{eq} (red diamonds) and fit parameters p_0 and q_0 (black symbols).

IV. CONCLUSION

In this work, quantitative measurements are performed of force-induced bond dissociation in an associative polymer gel under shear flow. These results provide an experimental measure to test the predictions of transient network theory that was not previously available. The small number of dissociated bonds even at large deformation suggests that retraction of dangling chains is insufficient to account for the shear thinning observed and highlights the importance of other modes that could lead to stress relaxation. It is hoped that the findings discussed here will aid in the advancement of the formulations of transient network theory and improve understanding of the molecular origin of shear thinning in associative polymer gels.

ACKNOWLEDGMENTS

This work was supported in part by the MRSEC Program of the National Science Foundation under Award No. DMR-1419807, the National Science Foundation under Award No. DMR-1709315, the U.S. Army Research Office through the Institute for Soldier Nanotechnologies under Contract No. W911NF-07-D-0004, and the Office of Naval Research (ONR) under the Young Investigators Program Grant ONR.N00014-15-1-2763.

[1] C. H. Li, C. Wang, C. Keplinger, J. L. Zuo, L. Jin, Y. Sun, P. Zheng, Y. Cao, F. Lissel, C. Linder, X. Z. You, and Z. Bao, Nat. Chem. **8**, 618 (2016).
[2] B. C. Tee, C. Wang, R. Allen, and Z. Bao, Nat. Nanotechnol. **7**, 825 (2012).
[3] G. E. Sanoja, N. S. Schauser, J. M. Bartels, C. M. Evans, M. E. Helgeson, R. Seshadri, and R. A. Segalman, Macromolecules **51**, 2017 (2018).
[4] Q. Zhang, S. Niu, L. Wang, J. Lopez, S. Chen, Y. Cai, R. Du, Y. Liu, J.-C. Lai, and L. Liu, Adv. Mater. **30**, 1801435 (2018).
[5] S. Bode, L. Zedler, F. H. Schacher, B. Dietzek, M. Schmitt, J. Popp, M. D. Hager, and U. S. Schubert, Adv. Mater. **25**, 1634 (2013).
[6] G. Scheltjens, M. M. Diaz, J. Brancart, G. Van Assche, and B. Van Mele, React. Func. Polym. **73**, 413 (2013).
[7] M. J. Glassman and B. D. Olsen, Soft Matter **9**, 6814 (2013).
[8] M. Guvendiren, H. D. Lu, and J. A. Burdick, Soft Matter **8**, 260 (2012).
[9] D. A. Z. Wever, F. Picchioni, and A. A. Broekhuis, Prog. Polym. Sci. **36**, 1558 (2011).
[10] K. C. Taylor and H. A. Nasr-El-Din, J. Pet. Sci. Eng. **19**, 265 (1998).
[11] S. C. Grindy, M. Lenz, and N. Holten-Andersen, Macromolecules **49**, 8306 (2016).
[12] D. E. Fullenkamp, L. He, D. G. Barrett, W. R. Burghardt, and P. B. Messersmith, Macromolecules **46**, 1167 (2013).
[13] P. Kord Forooshani and B. P. Lee, J. Polym. Sci., Part A **55**, 9 (2017).
[14] W. Wang, Y. Zhang, and W. Liu, Prog. Polym. Sci. **71**, 1 (2017).
[15] R. D. Groot, A. Bot, and W. G. Agterof, J. Chem. Phys. **104**, 9220 (1996).
[16] D. Xu, J. L. Hawk, D. M. Loveless, S. L. Jeon, and S. L. Craig, Macromolecules **43**, 3556 (2010).
[17] F. Tanaka and S. F. Edwards, J. Non-Newtonian Fluid Mech. **43**, 247 (1992).

[18] F. Tanaka and S. F. Edwards, J. Non-Newtonian Fluid Mech. **43**, 273 (1992).
[19] F. Tanaka and S. F. Edwards, J. Non-Newtonian Fluid Mech. **43**, 289 (1992).
[20] F. Tanaka and S. F. Edwards, Macromolecules **25**, 1516 (1992).
[21] S. Q. Wang, Macromolecules **25**, 7003 (1992).
[22] G. Marrucci, S. Bhargava, and S. L. Cooper, Macromolecules **26**, 6483 (1993).
[23] A. Vaccaro and G. Marrucci, J. Non-Newtonian Fluid Mech. **92**, 261 (2000).
[24] A. Tripathi, K. C. Tam, and G. H. McKinley, Macromolecules **39**, 1981 (2006).
[25] M. K. Sing, Z. G. Wang, G. H. McKinley, and B. D. Olsen, Soft Matter **11**, 2085 (2015).
[26] A. K. Omar and Z. G. Wang, Phys. Rev. Lett. **119**, 117801 (2017).
[27] B. V. K. J. Schmidt, M. Hetzer, H. Ritter, and C. Barner-Kowollik, Macromolecules **44**, 7220 (2011).
[28] F. S. Dainton and W. D. Sisley, Trans. Faraday Soc. **59**, 1385 (1963).
[29] S. Durmaz and O. Okay, Polymer **41**, 3693 (2000).
[30] See Supplemental Material at http://link.aps.org/supplemental/10.1103/PhysRevMaterials.4.055602 for calculation and experimental details.
[31] R. H. Holyer, C. D. Hubbard, S. F. A. Kettle, and R. G. Wilkins, Inorg. Chem. **5**, 622 (1966).
[32] S. M. Munzert, G. Schwarz, and D. G. Kurth, Inorg. Chem. **55**, 2565 (2016).
[33] M. Rubinstein and A. N. Semenov, Macromolecules **34**, 1058 (2001).
[34] A. J. Barlow, G. Harrison, and J. Lamb, Proc. R. Soc. A **282**, 228 (1964).
[35] J. D. Ferry and J. D. Ferry, *Viscoelastic Properties of Polymers* (Wiley, New York, 1980).
[36] T. Indei and J. Takimoto, J. Chem. Phys. **133**, 194902 (2010).
[37] J. Mewis, B. Kaffashi, J. Vermant, and R. J. Butera, Macromolecules **34**, 1376 (2001).
[38] L. Pellens, R. G. Corrales, and J. Mewis, J. Rheol. **48**, 379 (2004).